Chapter 5

Raman Effect and Magnetic Properties of doped $TbMnO_3$

5.1 Introduction

The preparation of material with simultaneous ferroelectricity and magnetic ordering would be a milestone for modern electronics and functionalized materials. Historically, magnetism and ferroelectricity are mutually exclusive phenomena by their mechanism of origin. The origin of magnetism is due to the presence of localized electrons in the partially filled d or f sub-shells in transition metal ions or rare earth ions, respectively, which has corresponding localized spins and magnetic moments, whereas most of the ferroelectrics have empty d sub-shells. This is the main reason for getting very few single-phase multiferroics. On the other hand, the magnetoelectric multiferroic materials provide the opportunity to encode information in electric polarization and magnetization to obtain four logic states.[1, 2] This makes these materials very promising for industrial applications such as new devices in information storage. In this respect, the study of RMnO$_3$ (R = Gd, Tb, Dy, Ho) is of considerable current interest owing to the co-existence of magnetic ordering and ferroelectricity with a strong coupling between them.[3–7]The ordering of the R spins below $T_N^R$is strongly dependent on the relative strengths of exchange interactions between Mn and R ions, $J_{Mn–R}$and between rare earths themselves, $J_{R–R}$[8].If the exchange interaction between Mn and rare earth (R) ions is weak then the R-ordering will not be affected much.[9, 10]On the other hand, strong $J_{Mn–R}$will force the R-ordering to the same periodicity as Mn down to the lowest temperatures.[11, 12]Moreover, a decrease in ionic radius of the R enhances the competition in magnetic interactions, i.e. ferromagnetic between nearest neighbouring Mn sites and AF between next nearest neighbouring sites.[13] The $TbMnO_3$ is in the intermediate coupling region and as a matter of fact it is the most interesting material[8] and has widely been studied.[14–21] This $TbMnO_3$ shows antiferromagnetic ordering and ferroelectric below 27 K.[5] Mn^{3+} magnetic moments order at T_{Mn} = 41 K while Tb^{3+} magnetic moments do so at T_{Tb} = 10 K. The frustrated spiral spin order of Mn^{3+} in $TbMnO_3$ is thought to be at the origin of the appearing ferroelectricity.[22] Also, the Tb and Mn orderings remain coupled down to the lowest temperatures through the harmonic coupling of their wave vectors. This is due to the minimization of the system's energy by adjusting the Ising type Tb spins to periodic Mn-ordering which leads to rather complex Tb-spin structure at low temperatures.[8] This intermediate coupling regime is very sensitive to any variation in $J_{Mn–R}$which strongly affects the Tb-magnetic ordering as has been observed by Prokhnenko *et al.*[23]

In this chapter, we have investigated the room temperature Raman scattering and temperature variation of magnetic properties of $Tb_{1-x}Y_xMnO_3$ and $TbMn_{1-x}Ni_xMnO_3$. The doping on different sites will effect the magnetic, electrical and structural properties which may provide the insight mechanism of this $TbMnO_3$ multiferroic. Substitution of both Tb^{3+} and Mn^{3+} will provide the variation of $J_{R-R}$and J_{Mn-Mn} and consequently J_{Mn-R}keeping J_{Mn-Mn} and J_{R-R}, respectively, fixed. Moreover, this study will further shed light on the effect of doping on different lattice sites of $TbMnO_3$.

5.2 Experimental

The doped- and undoped-$TbMnO_3$-polycrystalline samples were synthesized by the conventional solid state reaction technique. Stiochiometric amounts of Tb_4O_7, MnO, NiO and Y_2O_3 (all are of 99.99% purity) were mixed and followed a process given in below flow chart. All doped samples were synthesized by the same procedure. Single phase of the samples was characterized by an x-ray diffractometer (Model: MiniFlex II, Rigaku, Japan) with Cu Kα radiation (λ = 1.5406 Å). Magnetic measurement was carried out by SQUID (MPMS) magnetometer, Quantum Design. Raman spectra were taken with a Renishaw micro-Raman spectroscope using the 514.5 nm Ar^+ laser as excitation source.

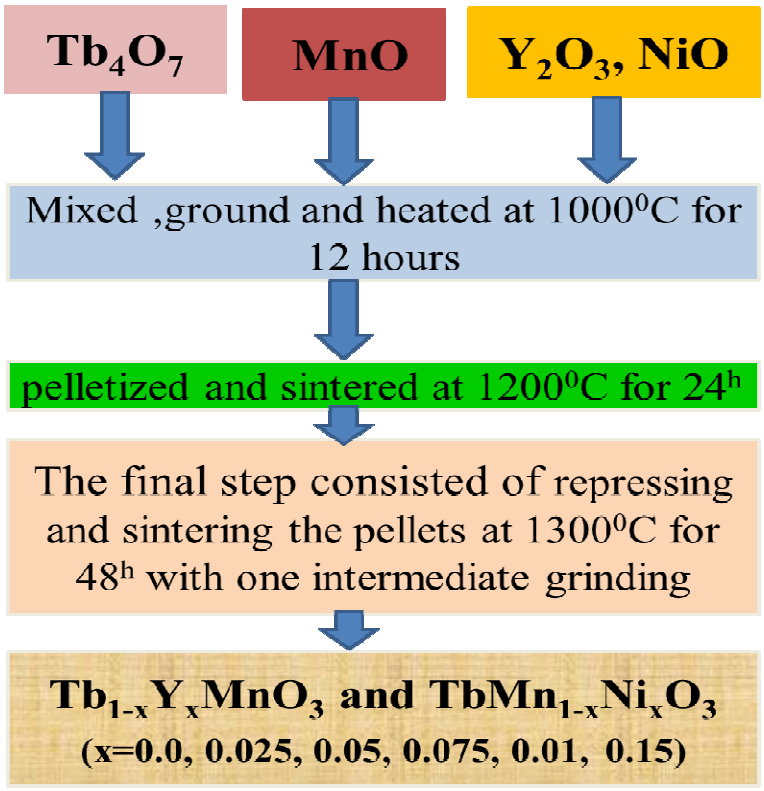

5.3 Results and Discussion

5.3.1 X-Ray Diffraction Study

Figure 5.1 shows the x-ray diffraction pattern of the Y- and Ni-doped $TbMnO_3$ samples which clearly indicates that all the compositions are of single phase. Figures 5.1(*a*) and (*b*) show the experimental, calculated and difference XRD patterns for $Tb_{1-x}Y_xMnO_3$ and $TbMn_{1-x}Ni_xMnO_3$ (x = 0, 0.05, 0.1, 0.15), respectively.

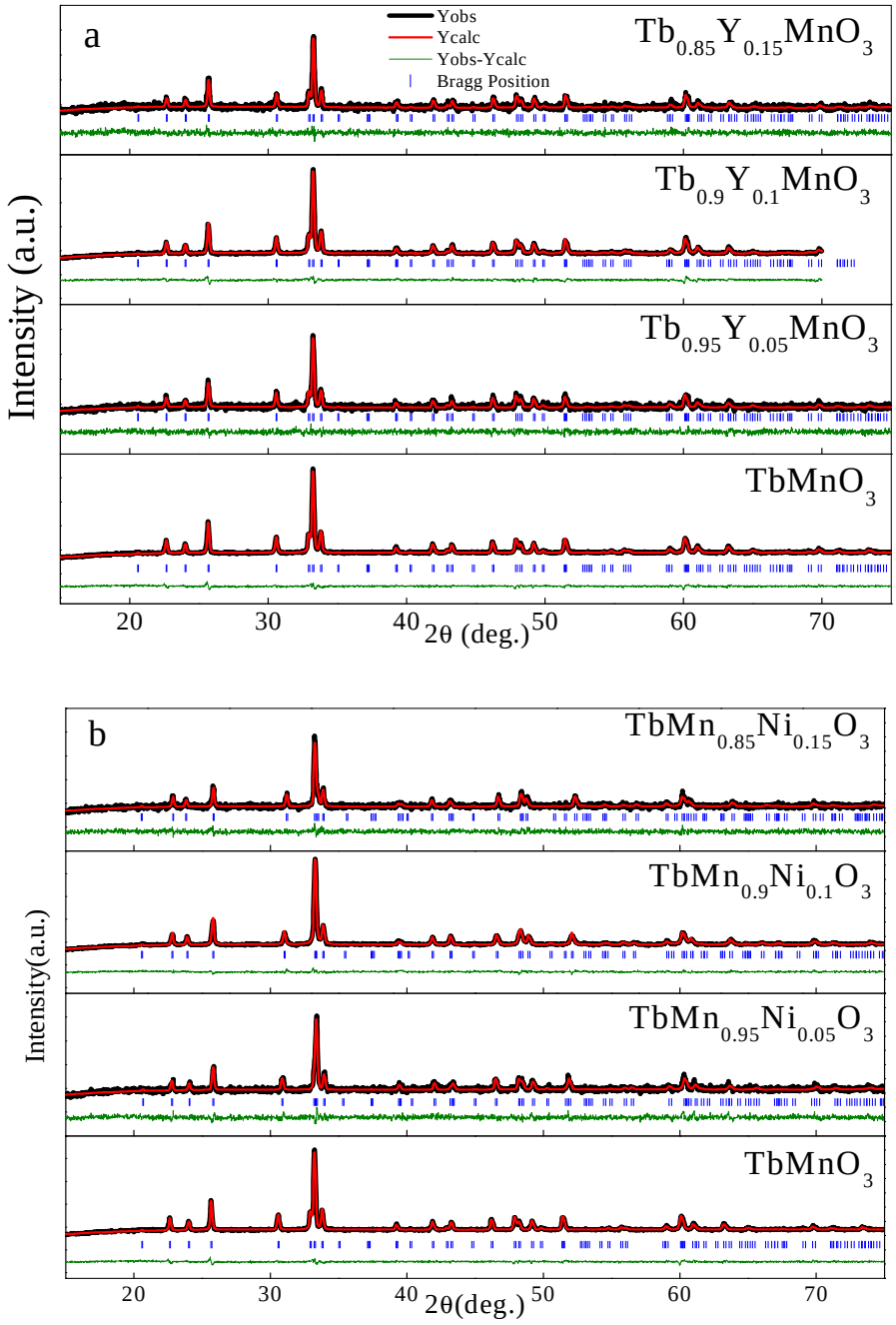

Figure 5.1 *X-ray diffraction pattern of $Tb_{1-x}Y_xMnO_3$ (a) and $TbMn_{1-x}Ni_xO_3$ (b). The Rietveld refinement fittings are also shown taking the Pbnm pace group.*

Table 5.1. *Crystal structure parameters for $Tb_{1-x}Y_xMnO_3$ obtained fromthe Rietveld refinements of powder x-ray diffraction* ***atroom*** *temperature using 1.5406 Å x-ray beam. The atom positions are given for Pbnm settings where Mn occupies 4b (1/2 0 0), Tb and O1 4c (x y 1/4), and O2 8d (x y z) Wyckoff positions.*

Parameter/Sample	$TbMnO_3$	$Tb_{0.95}Y_{0.05}MnO_3$	$Tb_{0.9}Y_{0.1}MnO_3$	$Tb_{0.85}Y_{0.15}MnO_3$
a (Å)	5.303 00(18)	5.3014(7)	5.299 95(19)	5.2969(5)
b (Å)	5.845 80(20)	5.845 84	5.843 70(20)	5.8407(6)
c(Å)	7.409 40(20)	7.4079(10)	7.407 70(20)	7.4033(7)
Mn–O1	1.9308(59)	1.9364(155)	1.9350(61)	1.9592(140)
Mn–O2	1.8996(163)	1.8329(363)	1.9056(164)	1.8302(418)
Mn–O2	2.2185(170)	2.3181(354)	2.2032(171)	2.2687(412)
Mn–O2–Mn (Å)	146.7(7)	143.6(14)	147.4(7)	148.0(17)
Mn–O1–Mn (Å)	147.2(2)	146.0(6)	146.3(3)	141.7(6)
Tb–O1	3.599(18)	3.53(5)	3.587(18)	3.68(5)
Tb–O1	2.384(18)	2.47(5)	2.406(18)	2.34(5)
Tb–O1	3.14(2)	3.16(5)	3.15(2)	3.23(4)
Tb–O1	2.31(2)	2.26(5)	2.29(2)	2.25(4)
Tb–O2	2.507(16)	2.55(3)	2.519(16)	2.50(4)
Tb–O2	2.590(14)	2.59(3)	2.567(15)	2.58(4)
Tb–O2	2.341(16)	2.28(3)	2.353(16)	2.36(4)
Tb-O2	3.641(16)	3.71(3)	3.629(16)	3.63(4)
R_F	2.19	5.60	2.20	5.56
χ^2	1.45	2.30	1.55	2.32

Table 5.2*Crystal structure parameters for $TbMn_{1-x}NixO_3$ obtained from the Rietveld refinement.*

Parameter/sample	$TbMnO_3$	$Tb_{0.95}Ni_{0.05}MnO_3$	$TbMn_{0.9}Ni_{0.1}O_3$	$Tb_{0.85}Ni_{0.15}MnO_3$
a(Å)	5.303 00(18)	5.2816(5)	5.292 20(19)	5.2925(5)
b(Å)	5.845 80(20)	5.7933(7)	5.763 70(20)	5.7328(6)
c(Å)	7.409 40(20)	7.3979(7)	7.4449(3)	7.4672(7)
Mn–O1	1.9308(59)	1.956(16)	1.9458(62)	1.9325(162)
Mn–O2	1.8996(163)	1.90(3)	1.9342(146)	1.9579(380)
Mn–O2	2.2185(170)	2.19(3)	2.1309(128)	2.1077(393)
Mn–O2–Mn (Å)	146.7(7)	146.6(12)	148.5(6)	147.3(15)
Mn–O1–Mn (Å)	147.2(2)	142.0(7)	146.1(3)	150.0(7)
Tb–O1	3.599(18)	3.68(6)	3.53(2)	3.55(6)
Tb–O1	2.384(18)	2.29(6)	2.38(2)	2.30(6)
Tb–O1	3.14(2)	3.20(5)	3.15(2)	3.06(6)
Tb–O1	2.31(2)	2.28(5)	2.28(2)	2.39(6)
Tb–O2	2.507(16)	2.44(3)	2.489(14)	2.51(4)
Tb–O2	2.590(14)	2.65(3)	2.597(14)	2.60(4)
Tb–O2	2.341(16)	2.32(3)	2.361(13)	2.32(4)
Tb–O2	3.641(16)	3.61(3)	3.572(13)	3.58(4)
R_F	2.19	5.14	2.00	5.06
χ^2	1.45	2.09	1.23	1.84

All the observed peaks can be fitted with the reflection conditions in the orthorhombic *Pbnm* space group. The final structural parameters and selected bond lengths and angles

are listed in tables 5.1 and 5.2. As seen from table 5.1, the Rietveld analysis afforded sufficiently low *R* factors.The lattice parameters, as well as the unit cell volume, are plotted as a function of Y and Ni concentration in figures 2(*a*) and (*b*), respectively.

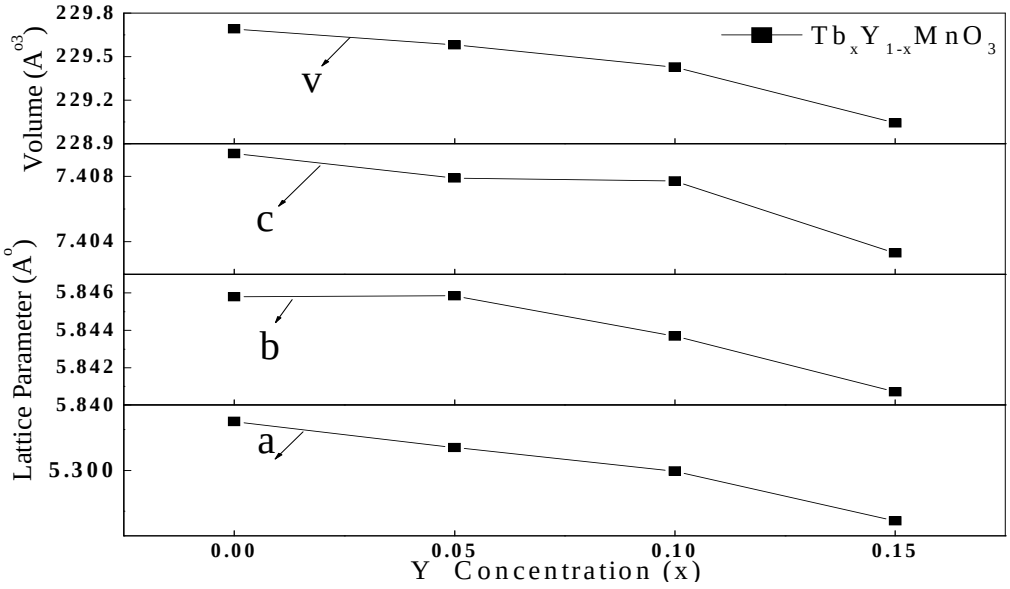

(a)

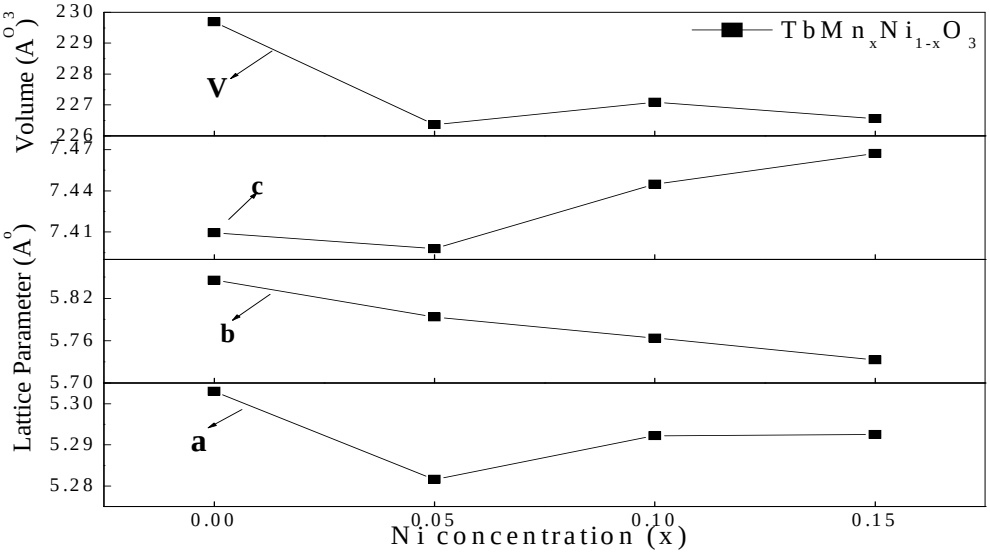

(b)

Figure 5.2: *Variation of lattice parameters with doping concentration of $Tb_{1-x}Y_xMnO_3$ (a) and $TbMn_{1-x}Ni_xO_3$ (b).*

With Y doping, the decrease in the two basal plane lattice parameters (*a*- and *b*-axes), and in the axial one (*c*-axis), result in the cell volume becoming smaller. It is well known that the ionic radius of Y^{3+} is smaller (1.04 Å) than that of Tb^{3+} (1.06 Å). Therefore, the decrease in cell volume upon Y doping is caused by the size effect. The

similar variation of cell volume has been reported for Sn-doped $TbMnO_3$.[14] On the other hand, when Ni is doped, the *c*-axis increases but the *a*- and *b*-axes decrease, which results in the decrease in cell volume. When Na^+ is doped, being larger in size than Tb^{3+},[24] the cell volume also decreases in a similar way. But in that case the decrease in cell volume is due to oxygen deficiency. Furthermore, the spontaneous orthorhombic strain, defined as $s = 2(b - a)/(a + b)$, which is also a measure of the distortion of the octahedral, increases as a result of octahedral tilting.[25] The estimated *s* value (0.097) of $TbMnO_3$ is in agreement with that reported by Alonso *et al* (s = 0.098).[26] In our case, the *s* value increases very slightly or remains constant with increasing Y and Ni content, which indicates that there is almost no change in the octahedral distortion and JT effect. The change in the lattice leads to an increase in the Mn–O–Mn bond angle: larger in the Ni-doping sample than the Y-doping one. A similar bond angle change is also observed in $SmMnO_3$ when Y is doped.[21] Both Tb site and Mn site doping change the Tb–O and Mn–O interatomic distances (presented in tables 5.1 and 5.2).

5.3.2 Analysis of Magnetic Properties

The temperature variations of the zero-field-cooled (ZFC) and field-cooled (FC) dc magnetization of $Tb_{1-x}Y_xMnO_3$ and $TbMn_{1-x}Ni_xO_3$ (x = 0.025, 0.05, 0.075, 0.10, 0.15) measured at 100 Oe are plotted in figures 5.3 and 5.4, respectively.

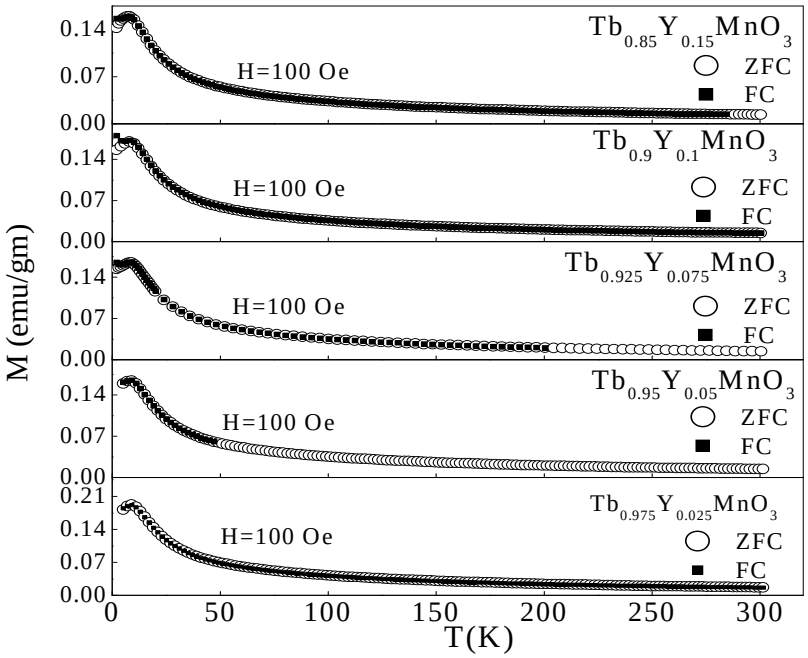

Figure 5.3: *Temperature variation of magnetization (field-cooled and zero-field-cooled) of $Tb_{1-x}Y_xMnO_3$.*

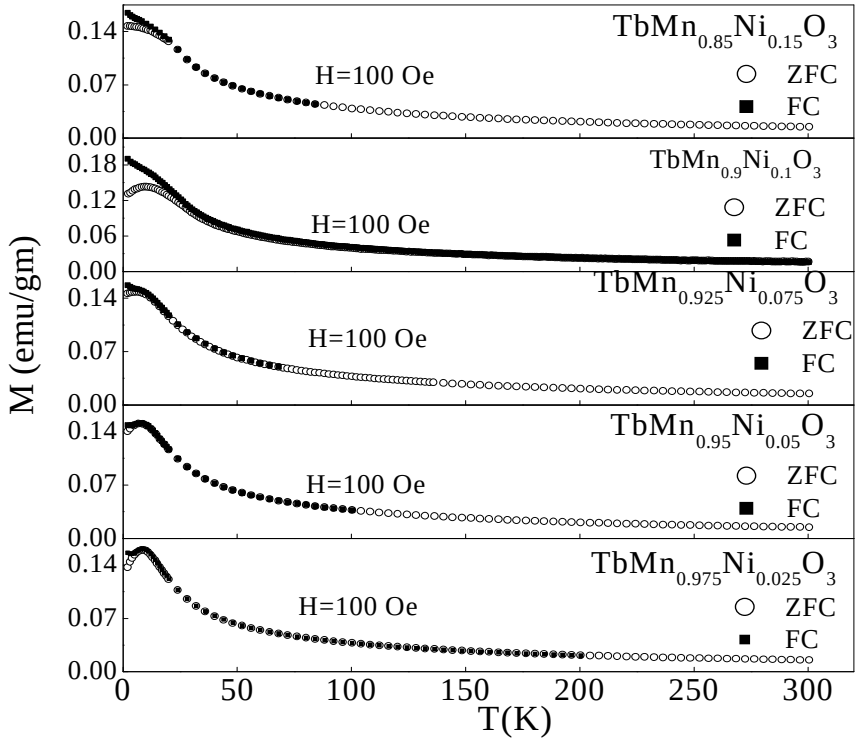

Figure 5.4:*Temperature variation of magnetization (field-cooled and zero-field-cooled) of $TbMn_{1-x}Ni_xO_3$.*

At low temperatures a bifurcation between FC and ZFC curves is found for both series of the samples below the irreversibility temperature T_{irr}. But for Y-doped samples the bifurcation is observed for the doping content greater than 0.05, whereas for the Ni-doped samples it is observed from the minimum doping concentration (0.025). The bifurcation is observed because $TbMnO_3$ is a frustrated system. On the other hand, with Ni doping, the bifurcation is more pronounced, which is due to the fact that Ni is doped on the magnetic Mn site. The temperature dependence of magnetization exhibits anomalies at the Neel´ temperature, T_N (T_N^{Mn}). The estimated Neel temperatures for both the Y-doped and Ni-doped samples are shown in table 6.3. The temperature dependences of magnetization of all the samples show a maximum at lower temperature, which indicate the proper antiferromagnetic ordering of the magnetic moments of terbium (T_N^{Tb}). It is observed that substitution of Tb by Y leads to the reduction in both T_N^{Mn} and T_N^{Mn}, whereas the substitution of Mn by Ni leads to reduction in T_N^{Mn}only. This is direct evidence of the effective reduction in both $J_{Tb–Mn}$ and $J_{Mn–Mn}$ when Y is doped and the reduction only in $J_{Mn–Mn}$ when Ni is doped. The decrease in T_N^{Mn} is observed when Sn is doped in $TbMnO_3$.[17] It has also been reported

that when Ga is doped in $TbMnO_3$ both the T_N^{Mn} and T_N^{Tb}[23] decrease as is observed in our Ni-doped samples. Figures 5.5(*a*) and (*b*) show the field dependence of the magnetization of $Tb_{1-x}Y_xMnO_3$ and $TbMn_{1-x}Ni_xO_3$. The coercive fields for different doping levels are estimated and shown in table 5.3. According to the figure, the curve for $TbMnO_3$ indicates the antiferromagnetic behavior.

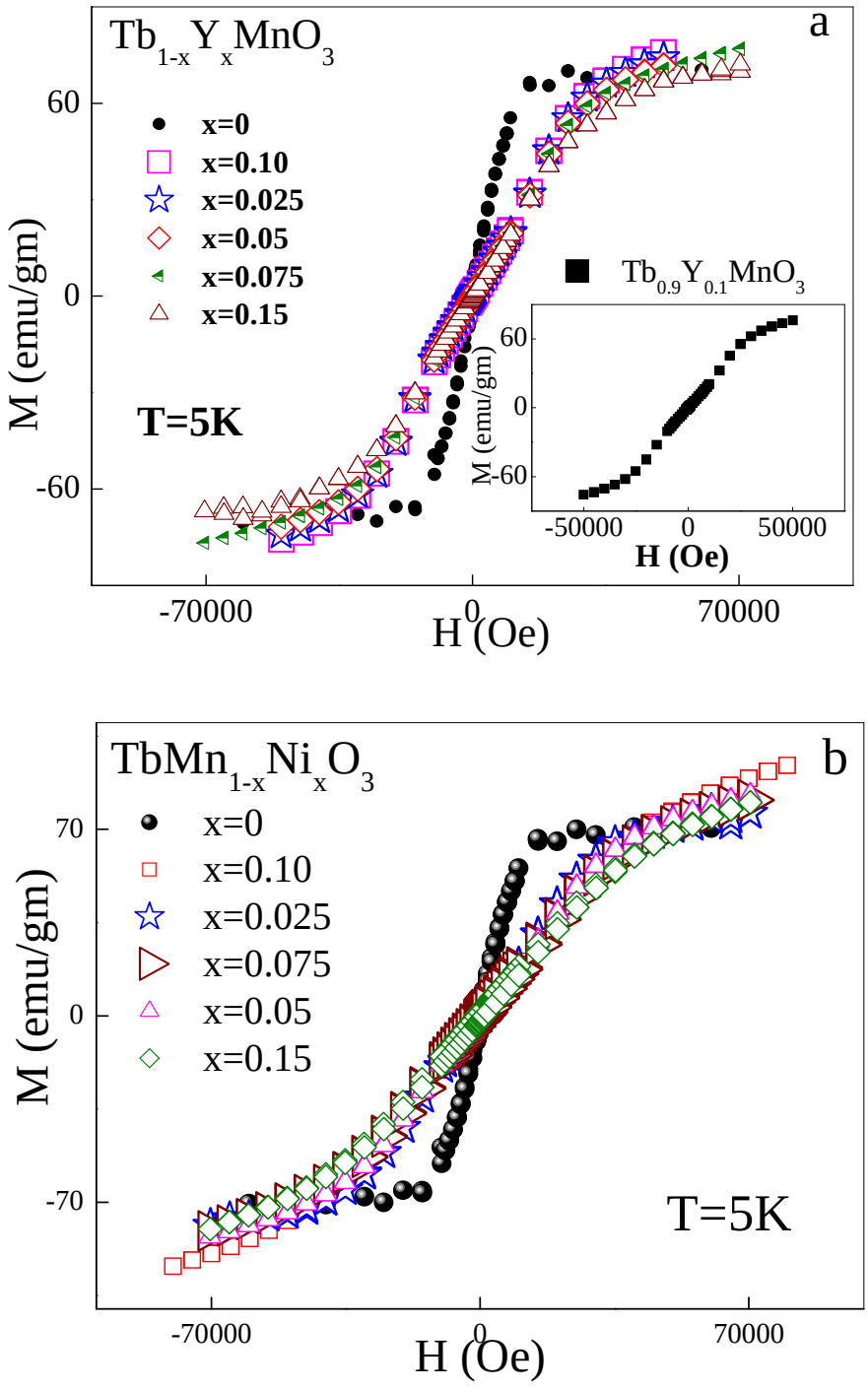

Figure 5.5: *Magnetization as a function of magnetic field (M–H hysteresis) of $Tb_{1-x}Y_xMnO_3$ (a) and $TbMn_{1-x}Ni_xO_3$ (b). The inset shown the M(H) of $Tb_{0.9}Y_{0.1}$ MnO_3.*

Table 5.3. Different magnetic parameters obtained from the *M(T)* and *M(H)* curves.

Parameter/Sample	Y0.025/Ni0.025	Y0.05/Ni0.05	Y0.075/Ni0.075	Y0.1/Ni0	Y0.15/Ni0.15
T_N^{Tb} (K)	8.8/9.2	7.7/8.2	7.7/8.2	6.8/9.2	5.8/9.2
T_N^{Mn} (K)	28.6/27.7	26.6/25.7	24.6/22.7	22.5/21.2	21.5/19.8
Coercive Field (Oe)	102/50	117/125	125/200	101/800	110/1000

It is observed that the $Tb_{0.9}Y_{0.1}MnO_3$ exhibits two critical magnetic fields corresponding to the suppression of the antiferromagnetic order on Tb ions and the reorientation of spins. This behaviour is consistent with that reported by Ivanov *etal* for single crystal.[27] The dilution of Tb by Y which has a slightly different ionic radius, obviously results in the smearing of the phase transitions. It is observed that with both Y and Ni doping the antiferromagentic correlation increases. From the above discussed results it is observed that Y doping on the Tb site affects both $J_{Mn–Tb}$ and $J_{Mn–Mn}$ whereas the Ni doping only affects the $J_{Mn–Mn}$. Therefore, the induced Tb magnetic ordering is affected by the Y for Tb substitutions. But the effect of Ni doping on $J_{Mn–Mn}$ is much more pronounced than that of Y doping. It is observed that when Gd is doped in $TbMnO_3$ the difference in the magnetic configuration between Gd and Mn produces the complex phase transition phenomena.[19] On the other hand, 5% Ca doping on the Tb site results the partial breakdown of the spiral structure.[20] In the present investigation it is observed that when the magnetic Tb ion is substituted by non-magnetic Y ion the magnetic ordering of the Mn sublattice is changed. This is consistent with the observation made by Prokhenko *et al* that the substitution of magnetic by non-magnetic ions in one of the sublattices can change the magnetic ordering in the other sublattice.[23] The reduction in $J_{Mn–Tb}$ also shows that Mn-exchange fields are involved in Tb-magnetic ordering in $TbMnO_3$ even belowT_N^{Tb}. It might be the case that the exchange field between Mn ions and the neighbouring Y ions is smaller than Tb sublattice. As a matter of fact $J_{Mn–Tb}$ decreases which in effect reduces the $J_{Mn–Mn}$. On the other hand, interestingly it is observed that $J_{Mn–Mn}$ decreases strongly with substitution of Mn by magnetic Ni but $J_{Mn–Tb}$ remains unaffected. The Neel temperature could´ be understood in terms of its relation with a spin exchange integral. For this, Mn^{3+} ions network can be adopted where Mn^{3+} ions are assumed to form a perfectly hexagonal network and each Mn^{3+} ion has six nearest neighbours. The Neel´ temperature T_N can be approximately related to the spin exchange integral J as $T_N = 0.3J(S + 1/2)^2$.[28] For

Mn^{3+}, S = 2 and the T_N will become 1.88J, whereas for Ni^{2+}, S = 3/2 and T_N will be 1.80J. The decrease in T_N is ~5%. But in the present investigation, Ni doping reduces the T_N by 8 K (much more than 5%). It might be the fact that Ni for Mn substitution does not correspond to homogeneous reduction in Mn–Mn exchange but the pronounced effects located at the sites which are occupied by Ni. It might be predicted that exchange interaction between Mn–Mn is opposite in nature to that of Mn–Ni which in effect decreases $J_{Mn–Mn}$. Furthermore, the exchange field of Tb ions in the near neighbourhood from Ni might be the same as that from Mn. It might be the fact that with Ni substitution the Tb-magnetic moments do not loose their alignment along *c* in the vicinity of Ni ions as has been predicted by Prokhenko *et al* for their Ga-doped samples.[23]

Moreover, it has also been reported by Jiang and Zhang[29] that when Mn site is doped the dopant valence and dopant radius play a crucial role in changing the local polarization. It has also been reported[29] that when divalent is doped the local polarization is always decreased. Therefore, Ni^{2+} doping might change the polarization flop observed in $TbMnO_3$[30] which in effect may change the exchange interaction.

5.3.3Raman Spectrum Study

Figures 6.6(*a*) and (*b*) show the room temperature Raman spectra of undoped and Y- and Ni-doped $TbMnO_3$ samples. The vibration modes in the $RMnO_3$ compounds are detected.[31–33] For $TbMnO_3$, there are 24 active Raman modes of ($7A_g + 7B_{1g} + 5B_{2g} + 5B_{3g}$). The different Raman modes of $RMnO_3$ as R for rare-earth ion mode are labelled T the tilt, A_g mode at between 280 and 370 cm^{-1}, AS for asymmetric stretch A_g mode at around 480 cm^{-1}, B the bending $A_g + B_{1g}$ mode between 420 and 530 cm^{-1} and SS for the symmetric stretch, B_{1g}, around 610 cm^{-1}.[24, 32, 34]No peak shift is observed when Y is doped but a small perturbation of the peak positions was found as Ni is increased for T, AS, B and SS modes, which originate from structural distortion. It was found that the sample showed four features labelled T, AS, B and SS at around 370 cm^{-1}, 479 cm^{-1}, 520 cm^{-1} and 610 cm^{-1}, respectively[34] and one second-order Raman scattering attributed mainly to the oxygen vibration mode at 650 cm^{-1}.[32]

It is known that the T, AS, B and SS modes depend on the Mn–O(1)–Mn angle, Mn–O(1) length, Mn–O(2) length and Tb–O length, respectively. We have plotted the doping concentration dependence of the Raman frequencies of the (a) tilt mode, (b)

bending modes and (c) stretching modes for both the systems (given in figure 7). The T, AS, B and SS features are indicated as A, B, C and D, respectively, in the figure. The T/A_g (4) normal mode is highly dependent on the tilt angle between the two octahedral. The bending mode which is assigned as B/Ag (3) + mixed (520 cm−1) includes two different A_g(3) normal modes indicating inside the MnO_6 octahedron, the angle between the O(1)–Mn–O(1) axis and the Mn–O(2) plane is bent, and the mixed modes are a combination of the A_g(3) and A_g(1) modes.

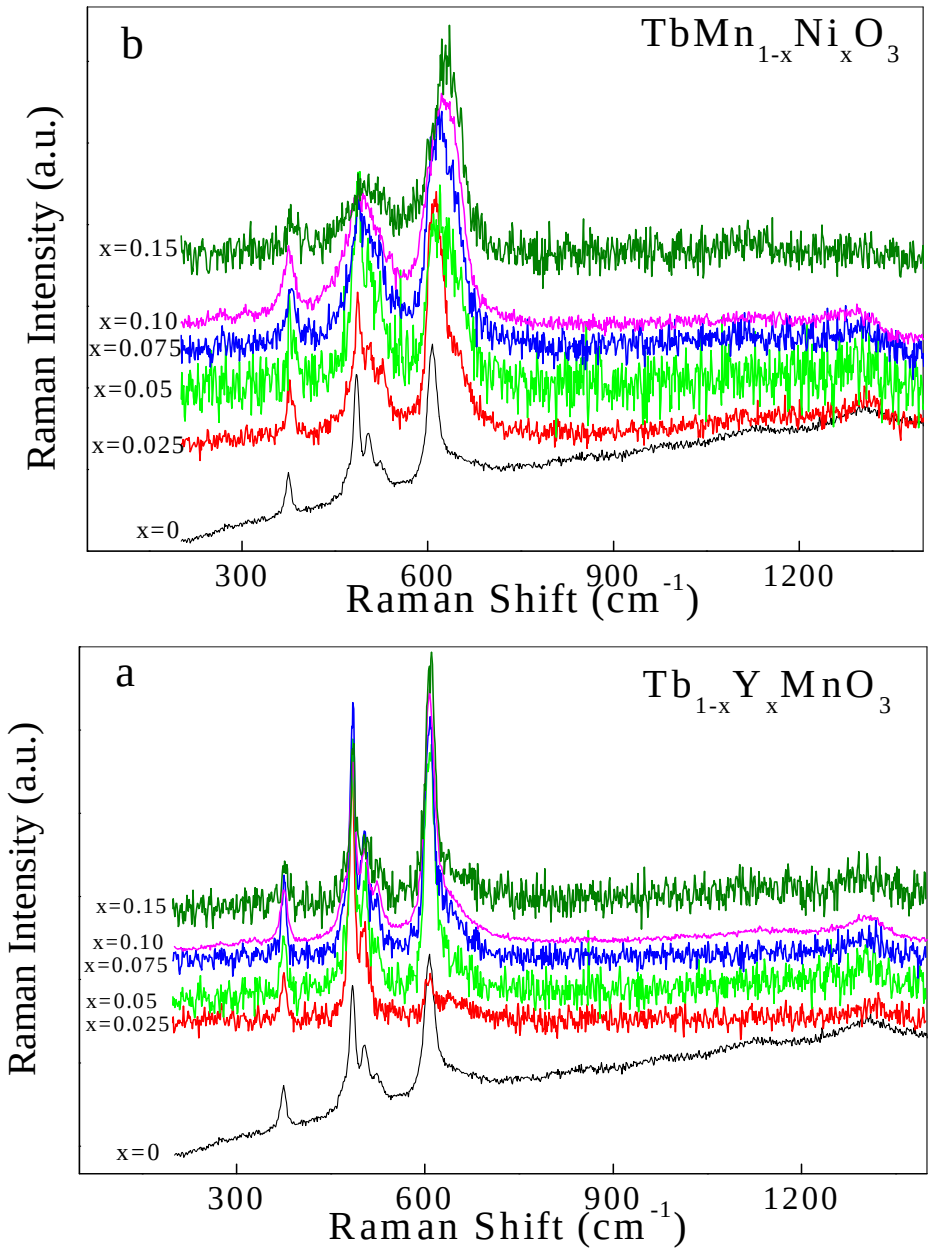

Figure 5.6: Raman spectra of $Tb_{1-x}Y_xMnO_3$ (*a*) and $TbMn_{1-x}Ni_xO_3$ (*b*).

Moreover, the Tb–O(1) bond length will bend the octahedron and bring about a larger force constant, indicating that higher frequency excitation is needed. The stretching

mode (symmetric and antisymmetric stretching) vibrates along the Mn–O bonds in- or out-of-phase. The in-phase term motions depend on shorter bond lengths/force constants and the out-of-phase term is the opposite. The features of Y-doped $TbMnO_3$ match with the low temperature Raman spectra of $TbMnO_3$ reported by Pradip Kumar *etal* [35] except the lower intensities of the peaks at higher frequencies (~1310 cm^{-1}). It is observed that when Y is doped on the Tb site almost no change in the spectrum is observed. But the intensity ratio (e.g. ratio of intensity at 608 cm^{-1} to the intensity at 370 cm^{-1}, i.e. I_{608}/I_{370}) increases when Y is doped. This is consistent with the observation made by Iliev *et al* [36]. The Y doping increases the distortion and decreases the bond lengths which lead to increase the Raman intensity. When Ni is doped on the Mn site the Raman spectrum changes: features at 485 and 608 cm^{-1} broaden and features at 506 and 527 cm^{-1} disappear. The modes at frequencies 485 cm^{-1} and 608 cm^{-1} are, respectively, due to MnO_6 bending and in-plane O_2 stretching. The frequency of a mode involving stretching vibrations of O_2 atoms in the *xz* planes is determined by the Mn–O_2 distances. In the present investigation when Ni is doped on the Mn site it is observed (table 5.2) that Mn–O(2) distances decrease which in effect broadens the modes at 485 and 608 cm^{-1}. This broadening should be a consequence of lattice disorder as induced by Ni doping on the Mn site.

5.4 Conclusion

The structural measurements show with Y doping '*b*' parameter decreases whereas, both '*a*' and '*c*' parameters remain almost constant or decrease very slightly which result in the decrease in unit cell volume. On the other hand, with Ni doping '*b*' parameter decreases and '*c*' parameter increases, whereas '*a*' parameter remains constant or decreases slightly. Both Y and Ni doping decrease the Neel temperature, T_N. Y doping reduces effectively both the $J_{Tb–Tb}$ and $J_{Mn–Mn}$ exchange interactions, whereas Ni doping on the Mn site decreases only the $J_{Mn–Mn}$ exchange interaction. The reduction in T_N in the Ni-doped sample cannot be explained with simple exchange integral where Mn^{3+} ions are assumed to form a perfectly hexagonal network. Ni^{2+} doping might change the polarization flop in $TbMnO_3$ which in effect may change the exchange interaction. In the room temperature Raman spectra for $TbMnO_3$ and Y-doped $TbMnO_3$, eight features are observed. When Ni is doped, modes due to MnO_6 bending and in-plane O_2 stretching broaden and few modes disappear. This might be due to the lattice disorder which is induced by Ni doping.

References:

[1]J. F. Scott, Nature Materials**6,** 256(2007).

[2]M. Gajek, M. Bibes Fusil, S. BouzehouaneKarim, J.Fontcuberta, A. Barthel´emy and A.Fert, Nature Mater.**6,** 296(2007).

[3]S.-W. Cheong and M.Mostovoy,Nature Mater.**6,** 13(2007).

[4]M.Pekala, V. Drozd, J. F.Fagnard, Ph.Vanderbemden and M. Ausloos J. Alloys Compounds**467,** 35(2007).

[5]T. Kimura, T.Goto, H. Shintani, K .Ishizaka, T. Arima and Y. Tokura, Nature**426 ,** 55 **(**2003).

[6]T. Goto, T.Kimura, G.Lawes, A.P.Ramirez and Y. Tokura, Phys. Rev. Lett.**92,** 257 **(**2004).

[7]B. Lorenz, Y.-Q. Wang and C.-W. Chu, Phys. Rev.B **76,**104405(2007).

[8]O. Prokhnenko, R.Feyerherm, M.Mostovoy, N.Aliouane, E.Dudzik, A. U. B.Wolter,A. Maljuk, and D. N. Argyriou Phys. Rev. Lett. **99,** 177206(2007).

[9]O. Prokhnenko, R. Feyerherm, E. Dudzik, S. Landsgesell, N. Aliouane, L. C. Chapon and D.N.Argyriou, Phys. Rev.Lett. **98,** 057206(2007).

[10] R. Feyerherm, E. Dudzik, N. Aliouane and D. N. Argyriou Phys. Rev. B **73,** 80401(2006).

[11] A. Munoz, M. T. Cas˜ ais, J. A. Alonso, M. J. Mart´ınez-Lope, J. L.Mart´ınez and M. T. Fernandez D´ıaz, Inorg. Chem.**40** 1020(2001).

[12] H. W. Brinks, J. Rodriguez-Carvajal, H. Fjellvag, A. Kjekshus and B. C.Hauback Phys. Rev.B **63,** 094411(2001).

[13] H. D. Zhou, J. C. Denyszyn and J. B. Goodenough, Phys.Rev. B **72** , 224401 (2005).

[14] Pekala, V. Drozd, J. F. Fagnard, Ph. Vanderbemden and M.Ausloos, J. Alloys Compounds**467,** 35(2009).

[15] Y. Y. Guo, Y. J. Guo, N. Zhang, L. Lin and J.-M.Liu,Appl.Phys.A **106,** 113(2012).

[16] P. Rovillain, M. Cazayous, Y. Gallais, A. Sacuto, M.-A. Measson and H. Sakata,Phys. Rev. B **81,** 054428(2010).

[17] F. W. Fabris, M. Pekala, V. Drozd, J. F Fagnard, Ph. Vanderbemden, S. Liu R and M. Ausloos, J. Appl.Phys **101,** 103904(2007).

[18] J.Blasco, C.Ritter, J.Gorcia, J. M. de-Teresa, J.Perez-Cacho and M. R.Ibarra Phys. Rev. B **62,** 5609(2000).

[19] T. Goto, Y.Yamasaki, H.Watanabe, T. Kimura and Y.Tokura Phys. Rev. B**72,** 220403 (2005).

[20] N.Mufti, A. A. Nugoroho, G. R.Blake and T. T. M. Palstra, Phys. Rev.B **78,** 024109(2008).

[21] D. O. Flynn, C. V. Tomy, M. R. Lees, A.Daoud-Aladin and G.Balakrishnan, Phys. Rev.B **83,** 174426(2011).

[22] M Mostovoy, Phys. Rev. Lett.**96,** 067601(2006).

[23] O. Prokhnenko, N.Aliouane, R.Feyerherm, E. Dudzik, A. U. B. Wolter, A. Maljuk, .Kiefer and D. N. Argyriou, Phys. Rev.B **81,** 024419(2010).

[24] T. S.Chan, R. S. Liu, C. C. Yang, W.-H.Li, Y. H.Lien, C. Y. Huang, J. W.Lynn, J. M.Chen and H.-S. Sheu, Inorg. Chem.**46,** 4575(2007).

[25] P. M. Woodward, T.Vogt, D. E. Cox, A.Arulraj, C. N. R.Rao, P.Karen and A. Cheetharm,Chem. Mater.**10,** 3652(1998).

[26] J. A .Alonso, M. J.Martinez-Lope, M. T. Casais and M. T. Fereundez-Diaz,Inorg. Chem.**39,** 917(2000).

[27] V. Yu .Ivanov, A. A. Mukhin, A. S. Prokhorov, A. M. Balbashov and L. D. Iskhakova,JETP Lett.**91,** 392(2010).

[28] N. T. Hien, S.-Y. Oh, X.-B. Chen, D. Lee, S.-Y. Jang, T. W. Nohc and I.-S. Yanga, J. Raman Spectrosc. **42,** 1774(2011).

[29] N. Jiang and X. Zhang, J. Phys.: Condens. Matter**24,** 235402(2012).

[30] Y.Yamasaki, S.Miyasaka, T. Goto, H.Sagayama, T.Arima and Y. Tokura, Phys. Rev. B **76,** 184418(2007).

[31] M. V. Abrashev, J. Backstr¨ om, L. B¨ orjesson, V. N.Popov,¨ R. A.Chakalov, N. Kolev, R.-L. Meng and M. N. Iliev, Phys. Rev.B **65,** 184301(2002).

[32] Mart´ın-Carron L, A. D.Andr´ es, M. J. Mart´ ´ınez-Lope, M. T. Casais and J. A.Alonso,Phys. Rev. B**66,** 174303(2002).

[33] M. N. Iliev, M. V. Abrashev, V. N. Popov and V. G. Hadjiev, Phys. Rev.B **67,** 12301(2003).

[34] B. V. Podobedov, A. Weber, D. B. Romero, J. P. Rice and H. D. Drew, Phys. Rev. B **58,** 43(1998).

[35] P. Kumar, S. Saha, D. V. S. Muthu, J. R. Sahu, A. K. Sood and C. N. R.Rao J. Phys.:Condens. Matter **22,** 115403(2010).

[36] M. N. Iliev, M. V. Abrashev, J. Laverdiere, S. Jandl, M. M .Gospodinov, Y-Q .Wang

and Y-Y. Sun, Phys. Rev.B **73,** 064302 (2006).